JOC The Journal of Organic Chemistry

Featured Article

pubs.acs.org/joc

C^8-Heteroaryl-2′-deoxyguanosine Adducts as Conformational Fluorescent Probes in the *Nar*I Recognition Sequence

Katherine M. Rankin,[†] Michael Sproviero,[†] Keegan Rankin,[‡] Purshotam Sharma,[§] Stacey D. Wetmore,*[,§] and Richard A. Manderville*[,†]

[†]Departments of Chemistry and Toxicology, University of Guelph, Guelph, Ontario N1G 2W1, Canada

[‡]Department of Chemistry, University of Toronto, Toronto, Ontario M5S 3E4, Canada

[§]Department of Chemistry & Biochemistry, University of Lethbridge, Lethbridge, Alberta T1K 3M4, Canada

Supporting Information

ABSTRACT: The optical, redox, and electronic properties of C^8-heteroaryl-2′-deoxyguanosine (dG) adducts with C^8-substituents consisting of furyl (^{Fur}dG), pyrrolyl (^{Pyr}dG), thienyl (ThdG), benzofuryl (^{Bfur}dG), indolyl (^{Ind}dG), and benzothienyl (^{Bth}dG) are described. These adducts behave as fluorescent nucleobase probes with emission maxima from 379 to 419 nm and fluorescence quantum yields (Φ_{fl}) in the 0.1−0.8 range in water at neutral pH. The probes exhibit quenched fluorescence with increased solvent viscosity and decreased solvent polarity. The ^{Fur}dG, ^{Bfur}dG, ^{Ind}dG, and ^{Bth}dG derivatives were incorporated into the G_3 position of the 12-mer oligonucleotide 5′-CTCG$_1$G$_2$CG$_3$CCATC-3′ that contains the recognition sequence of the *Nar*I Type II restriction endonuclease. This sequence is widely used to study the biological activity (mutagenicity) of C^8-arylamine−dG adducts with adduct conformation (*anti* vs *syn*) playing a critical role in the biological outcome. The modified *Nar*I(X = ^{Fur}G, ^{Ind}G, ^{Bfur}G, or ^{Bth}G) oligonucleotides were hybridized to the complementary strand containing either C (*Nar*I′(C)) or G (*Nar*I′(G)) opposite the probe. The duplex structures were characterized by UV melting temperature analysis, fluorescence spectroscopy, collisional fluorescence quenching studies, and circular dichroism (CD). The emission of the probes showed sensitivity to the opposing base in the duplex, and suggested the utility of fluorescence spectroscopy to monitor probe conformation.

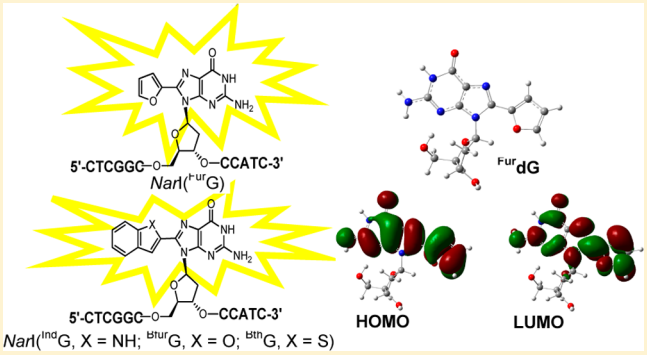

INTRODUCTION

Fluorescent nucleobase analogues have a wide range of applications that include use as reporters of nucleic acid structure and function;[1−3] investigating nucleobase damage;[4] detecting single nucleotide polymorphism (SNP);[5] understanding protein−DNA interactions,[6] generation of fluorescent aptasensors that provide an optical signal upon molecular target binding,[7] and use as oligonucleotide-based therapies.[8] The prototypical fluorescent base analogue is 2-aminopurine (2AP), which causes little perturbation to DNA structure.[9] The fluorescence of 2AP is strongly quenched when incorporated into single-strand oligonucleotides and quenched further still when hybridized to a complementary strand.[10] The decrease in quantum yield of 2AP also varies with oligonucleotide sequence, temperature, and helical conformation, and these characteristics have been exploited to understand structural dynamics,[11] protein−DNA interactions,[12] and charge transfer within duplex and hybrid (i.e., RNA:DNA) helical structures.[13,14]

Fluorescent nucleobase probes that retain high quantum yields upon oligonucleotide incorporation have also been developed.[15,16] Here, modified cytosine analogues with fused tricyclic ring systems have proven useful[17,18] and have been converted into fluorescence resonance energy transfer (FRET) pairs to distinguish between distance and orientation changes.[19] Attachment of aryl groups to the commercially available pyrrolo-dC[20] or to C^5 of deoxyuridine (dU)[21,22] has also been employed to generate solvent-sensitive emissive probes. Within this division of analogues, pyrimidine bases bearing heteroaryl ring systems (furan,[21] or benzothiophene[22]) show excellent photophysical properties for determining the microenvironment of the fluorescent probe.

Generation of emissive purine nucleobase probes has also attracted attention with the C^8 position being a usual site of modification.[23−29] However, in this case, the attachment of π-systems to generate emissive purine probes can shift the conformational equilibrium of the glycosidic bond from *anti* to *syn*.[23] When the C^8-modified purine adopts the *syn*-conformation, Watson−Crick (W−C) base pairing with its pyrimidine partner cannot take place and the probe can disrupt the helical structure. Under this scenario, the emissive

Received: October 2, 2012
Published: November 21, 2012

nucleobase is a poor model for the unmodified purine. Thus, in order to generate purine analogues that minimally disturb the structure and function of nucleic acids, a small vinyl group has been attached to C^8 of both dA[24] and dG,[25] and the resulting probes have been found to be nonperturbing with improved sensitivity over 2AP. Larger aromatic systems have also been attached to C^8 of dA[26] and dG[27−29] where dG derivatives are useful for monitoring G-quadruplex folding, since the preferred *syn*-conformation of the modified C^8-dG nucleobase can stabilize the G-tetrad.[28,29]

Our interest in C^8-aryl−dG adducts stems from their toxicological relevance. A number of chemical mutants generate radical species that undergo direct addition reactions at C^8 of dG to afford carbon (C)- and oxygen (O)-linked adducts.[30,31] These adducts are related, in terms of dG modification site, to nitrogen (N)-linked derivatives formed by arylamine[32] and heterocyclic aromatic amines[33] that are known human carcinogens. For N-linked adducts, the *syn*-conformation is regarded as promutagenic and plays a critical role in their biological activity.[32−35] These lesions are generally nonfluorescent, and therefore, analytical tools with generally lower limits of detection have been employed to distinguish conformation, including circular dichroism (CD),[36] UV absorption,[37] ^{19}F NMR,[38] and ^{1}H NMR[32,39] spectroscopies. However, for C-linked adducts where conformation is also expected to play an important biological role, fluorescence spectroscopy is an attractive alternative for probing conformational preference.

Recently, we used thermal melting (T_m) studies, CD, molecular dynamics (MD), and notably, fluorescence spectroscopy to study the conformational preferences of phenolic C-linked C^8-dG adducts in duplex DNA.[40] The use of fluorescence spectroscopy in defining adduct conformation did present limitations, as the excitation maximum of the adducts (∼280 nm) overlapped with that of natural DNA (∼260 nm). However, we have shown that the indole-linked (^{Ind}dG) C^8-dG nucleoside (Figure 1) can act as a fluorescent

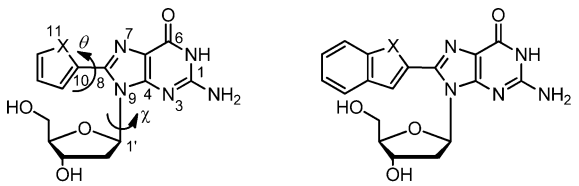

*Nar*I = 5'-CTCGGCXCCATC, X = ^{Fur}dG, ^{Ind}dG, ^{Bfur}dG or ^{Bth}dG
*Nar*I'(N) = 5'-GATGGNGCCGAG, N = C or G

Figure 1. Structures of C^8-heteroaryl−dG nucleosides and *Nar*I oligonucleotide sequence considered in the present study. The dihedral angle χ (∠(O4′−C1′−N9−C4)) defines the glycosidic bond orientation to be *anti* (χ = 180 ± 90°) or *syn* (χ = 0 ± 90°), and θ (∠(N9−C8−C10−X11)) defines the degree of twist between the nucleobase and the C^8-substituent.

reporter of *syn*- versus *anti*-structures on the basis of its sensitivity to H-bonding in aprotic solvents and possesses an excitation maximum (∼320 nm) distinct from DNA.[41] The benzothienyl derivative (^{Bth}dG, Figure 1) was also incorporated into two decanucleotide sequences and was found to act as an emissive conformational probe.[42] In this case, the reporting capability of ^{Bth}dG was ascribed to changes in π-stacking and charge-transfer character between the benzothienyl moiety with the natural DNA bases in the duplex structure.

We have now extended our studies on C^8-heteroaryl−dG adducts and have used density functional theory (DFT) calculations to help define the electronic and structural properties of both the 5-membered ring derivatives (^{Pyr}dG, ^{Fur}dG, and ThdG, Figure 1) and the bulkier benzoheterocyclic series of adducts (^{Ind}dG, ^{Bfur}dG, and ^{Bth}dG, Figure 1). The calculations provide a rationale for their photophysical properties in solvents of differing polarity and rigidity. The C^8-heteroaryl−dG adducts ^{2Fur}dG, ^{Ind}dG, ^{Bfur}dG, and ^{Bth}dG were incorporated into G_3 of the 12-mer oligonucleotide 5′-CTCG$_1$G$_2$CG$_3$CCATC that contains the recognition sequence of the *Nar*I Type II restriction endonuclease. This sequence was chosen for study because the G_3 site represents a "hotspot" for mutagenicity mediated by N-linked C^8-dG adducts.[33,35,39] Our goal is to derive structure−activity relationships for C^8-dG adducts, and emissive C^8-heteroaryl−dG probes that mimic the structural impact of C-linked adducts within duplex structures could thereby help elucidate mechanisms of mutagenesis through the use of luminescence-based assays.[42] The experiments described herein outline the role of the heteroatom (X) and size of the C^8-heteroaryl group in observing changes in probe microenvironment using fluorescence spectroscopy. This information has provided a deeper understanding of the reporting capabilities of these emissive probes.

RESULTS AND DISCUSSION

Structural, Photophysical, and Redox Properties of C^8-Heteroaryl−dG Adducts. The optical and redox properties of the C^8-heteroaryl−dG nucleoside adducts and unmodified dG[43] are given in Table 1. Absorption and emission spectra were recorded in aqueous MOPS buffer, while the redox properties were determined using cyclic voltammetry (CV) in anhydrous DMF, as outlined previously.[44−46] All C^8-heteroaryl−dG nucleoside adducts have lower 1-electron half-peak oxidation potentials ($E_{p/2}$) than dG, indicating that the heteroaryl moiety enhances the electron donor character of the purine nucleoside. The pyrrole-linked derivative ^{Pyr}dG possesses the lowest $E_{p/2}$ value of 0.78 V vs saturated calomel electrode (SCE), followed by ^{Ind}dG ($E_{p/2}$ =

Table 1. Photophysical and Redox Parameters for C^8-Heteroaryl−dG Adducts

adduct	λ_{max} (nm), log ε^b	λ_{em} (nm),^{b} $\phi_{fl}{}^c$	$\Delta\nu^d$ (cm^{-1})	brightness^e	$E_{p/2}{}^f$
^{Pyr}dG	292, 4.36	379, 0.10	7861	2291	0.78
^{Fur}dG	292, 4.31	384, 0.49	8205	10005	0.91
ThdG	284, 4.24	414, 0.79	11057	13729	1.05
^{Ind}dG	321, 4.48	390, 0.78	5512	23600	0.89
^{Bfur}dG	323, 4.41	405, 0.76	6268	19500	0.92
^{Bth}dG	315, 4.27	419, 0.46	7880	8570	1.06
dG^a	253, 4.14	334, 9.7 × 10^{-5}	9620	1.33	1.14

^{a}Photophysical data for dG taken from ref 43. ^{b}Determined in 10 mM MOPS buffer, pH 7, μ = 0.1 M NaCl. ^{c}Determined using the comparative method with quinine bisulfate in 0.5 M H_2SO_4 (ϕ_{fl} = 0.55). ^{d}Stokes shift ($\Delta\nu$) is calculated as $(1/\lambda_{max} - 1/\lambda_{em})$. ^{e}Brightness factor is calculated as $\varepsilon_{\lambda max} \times \phi_{fl}$. ^{f}Half-peak potentials in volts vs SCE using cyclic voltammetry with 0.1 M TBAF in anhydrous DMF using a glassy carbon working electrode.

dx.doi.org/10.1021/jo302164c | J. Org. Chem. 2012, 77, 10498−10508

0.89 V), which is closely followed by the oxygen-containing analogues (^{Fur}dG and ^{Bfur}dG ~0.92 V), and finally the sulfur-containing derivatives (ThdG, ^{Bth}dG ~1.05 V). This indicates that thienyl and benzothienyl substituents are the least electron-donating groups. The sulfur analogues also show the largest Stokes' shift ($\Delta\nu$), displaying blue-shifted absorption values and red-shifted emission wavelengths compared to the other nucleosides. In fact, a clear trend is apparent between $E_{p/2}$ and emission wavelength where increased $E_{p/2}$ values cause the emission to shift to longer wavelengths. The solvatochromic properties of the C^8-heteroaryl−dG nucleosides are given in Tables S1−S6 (Supporting Information (SI)). As previously presented for ^{Bth}dG,[42] the probes tend to show an increase in $\Delta\nu$ with increased solvent polarity, consistent with the excited state possessing a dipole moment greater than the ground state.[47]

Insight into the structural features and electronic properties of the C^8-heteroaryl−dG adducts was obtained from DFT calculations, as presented previously for ^{Pyr}dG, ^{Ind}dG,[41] and various C^8-Ar−dG adducts.[23,48] The C^8-heteroaryl−dG adducts adopt the *syn*-conformation, as predicted from their NMR chemical shifts in DMSO (Table S7, SI)[29] and from DFT calculations where all *syn* minima contain an O5′−H···N3 H-bond and are ~25 kJ mol^{-1} more stable than *anti* minima.[41] Fully optimized *syn* minima and transition states on the potential energy surfaces for the C^8-heteroaryl−dG adducts are displayed in Figures S1−S6 (SI). The degree of twist angle (θ) between the heteroaryl ring with respect to the nucleobase is dependent on the nature of the heteroatom X. For ^{Pyr}dG the twist angle θ is 14.4°, while θ for ThdG is ~32°, which is similar to θ calculated for ^{Bth}dG (~31°, Figure 2). The HOMO and LUMO of ^{Pyr}dG (Figure 2) consist of delocalized π orbitals with almost equal density on the nucleobase and pyrrole ring system. The HOMO of ^{Bth}dG also consists of delocalized π orbitals, while the LUMO has greater density on the benzothienyl ring system, which is consistent with push−pull

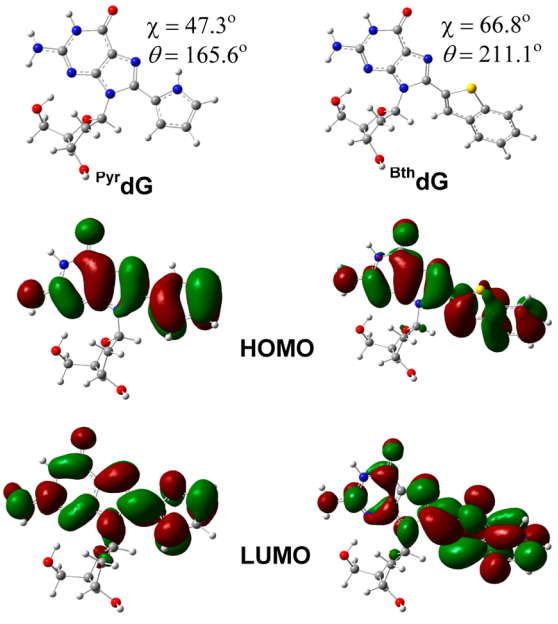

Figure 2. Ground-state B3LYP/6-31G(d) global minima and orbital density plots of ^{Pyr}dG and ^{Bth}dG. The HOMO and LUMO energy levels (eV) are given in Table 2.

character from the donor nucleobase to the acceptor C^8-substituent.[49]

Orbital energies for the C^8-heteroaryl−dG adducts obtained from the DFT calculations are summarized in Table 2. The

Table 2. Electronic Properties[a] of C^8-Heteroaryl−dG Adducts

adduct	HOMO E (eV)	LUMO E (eV)	ΔE calcd (eV)	V_{ex} E^b (eV)	ΔE optical (eV) [λ_{abs} (nm)][c]
^{Pyr}dG	−5.12	−0.52	4.60	4.16	4.20 [295]
^{Fur}dG	−5.32	−0.94	4.38	4.11	4.25 [292]
ThdG	−5.50	−1.09	4.41	4.04	4.32 [287]
^{Ind}dG	−5.24	−1.09	4.15	3.86	3.82 [325]
^{Bfur}dG	−5.35	−1.32	4.03	3.77	3.86 [321]
^{Bth}dG	−5.51	−1.33	4.18	3.83	3.86 [321]

[a]Optimized at the B3LYP/6-31G(d) level, with values corresponding to a ground state (S_0) with a relative energy of 0 kJ/mol. [b]Vertical excitation energy values determined from the corresponding TD-B3LYP/6-31G(d) calculations. [c]Determined experimentally for C^8-heteroaryl−dG adducts from UV absorption data in acetonitrile.

benzoheterocyclic series have lower HOMO−LUMO gaps than the 5-membered ring analogues, and TD-B3LYP/6-31G(d) vertical excitation energies (V_{ext}) tend to correlate better than the calculated HOMO−LUMO gaps with λ_{max} values determined in CH_3CN. Changes in structural and electronic (dipole moment) properties of the nucleoside probes from the ground state (S_0) to excited state (S_1), as predicted from DFT calculations, are given in Table 3. For all nucleosides, the

Table 3. Change in Structural Properties and Dipole Moments from Ground (S_0)[a] to Excited State (S_1)[b] of C^8-Heteroaryl−dG Adducts

adduct	χ (S_0)/χ (S_1) (deg)	θ (S_0)/θ (S_1) (deg)	μ (S_0)/μ (S_1) (Debye)
^{Pyr}dG	47.3/40.4	165.6/181.4	3.64/4.46
^{Fur}dG	50.1/48.5	343.8/0.16	4.27/4.86
ThdG	67.2/64.9	212.3/185.6	5.18/6.05
^{Ind}dG	46.9/44.4	166.5/178.9	4.83/5.63
^{Bfur}dG	49.9/49.8	345.6/359.7	4.37/5.08
^{Bth}dG	66.8/69.7	211.1/188.1	5.45/6.41

[a]Optimized at the B3LYP/6-31G(d) level, with values corresponding to a S_0 with a relative energy of 0 kJ/mol. Optimized at the CIS/6-31G(d) level, with S_1 state optimization starting from the corresponding S_0-state geometry.

calculations predict twisted S_0 structures that become almost planar ($\theta \sim 0, 180, 360°$) in S_1, which is consistent with the behavior of biphenyl systems.[50] All of the adducts possess greater dipole moments in S_1, which is consistent with their solvatochromic properties (Tables S1−S6, SI).[42] The sulfur analogues (ThdG and ^{Bth}dG) have the most twisted S_0 structures and the largest dipole moments in S_0 and S_1 states and show the greatest increase in dipole moment on going from S_0 to S_1. These properties provide a rationale for the photophysical parameters given in Table 1. Within each class of C^8-heteroaryl−dG nucleosides (5-membered rings and benzoheterocyclic series), the sulfur analogues have the most blue-shifted absorption spectra because they have the highest degree of twist in S_0 due to the larger S-atom. This disfavors conjugation between the nucleobase and the C^8-substituent. Upon conversion to a planar structure in S_1, the sulfur

dx.doi.org/10.1021/jo302164c | J. Org. Chem. 2012, 77, 10498−10508

derivatives have the most red-shifted emission, as they can accept electron density in their excited states and as a consequence the nucleosides have the greatest S_1 dipole moments.

The calculated properties of C^8-heteroaryl−dG adducts (Table 3) also provide a rationale for their changes in emission with increased solvent viscosity and temperature. Figure 3

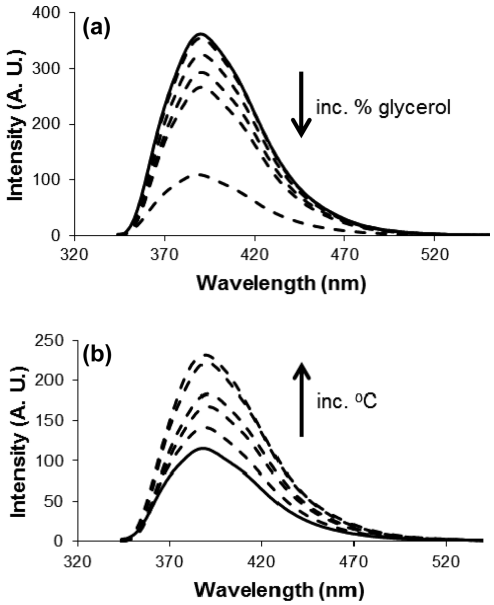

Figure 3. Changes in fluorescence emission spectra (dashed traces) of ^{Ind}dG upon (a) increasing the glycerol content from 0% (solid trace, 100% 10 mM MOPS, pH 7, μ = 100 mM NaCl) up to 100% (added in 20% increments), recorded at 20 °C, and (b) increasing the temperature in 10 °C increments from 20 °C (solid trace) in 100% glycerol.

shows changes in emission for ^{Ind}dG in glycerol−water mixtures at 20 °C (Figure 3a) and with increased temperature in 100% glycerol (Figure 3b). The spectral changes shown in Figure 3 for ^{Ind}dG are representative of emission changes for C^8-heteroaryl−dG nucleoside adducts, which show a 3−4-fold decrease in emission intensity from buffered water to 100% glycerol, accompanied by a blue-shift in emission wavelength of 2−6 nm. Increasing the temperature from 20 to 80 °C in 100% glycerol increases emission intensity 2−3-fold. With increased viscosity, excited states have geometries similar to that of the ground state,[51] because increased solvent rigidity increases barriers to rotation. Thus, a possible explanation for the emissive behavior of C^8-heteroaryl−dG nucleosides with increased viscosity and temperature could stem from the generation of twisted S_1 structures, which causes a blue-shift in emission wavelength and a decrease in intensity. Increased temperature in 100% glycerol decreases the barrier to rotation and more emissive planar structures in S_1 can be generated.

Synthesis of Modified *Nar*I. To test the emissive properties of these probes in a helical environment, the benzoheterocyclic series ^{Ind}dG, ^{Bfur}dG, and ^{Bth}dG along with the 5-membered derivative ^{Fur}dG were incorporated into the 12-mer *Nar*I sequence at the G_3 position (Figure 1). Our choice of these adducts stemmed from their photophysical properties given in Table 1. The bulky benzoheterocyclic series all exhibit excitation maxima distinct from DNA and permit the role of the heteroatom X to be determined. The excitation maxima of the 5-membered derivatives were expected to overlap with DNA. However, ^{Fur}dG has a red-shifted maximum compared to ThdG and was significantly brighter than ^{Pyr}dG. For this reason ^{Fur}dG[52] was chosen from the 5-membered derivatives and its incorporation into *Nar*I provides a direct comparison to ^{Bfur}dG in terms of ring size. Our choice of *Nar*I as the oligonucleotide substrate stems from its extensive use as a substrate for related N-linked C^8-dG adducts derived from arylamine carcinogens.[33,35,37,39]

The C^8-heteroaryl−dG adduct ^{Fur}dG was incorporated into *Nar*I using standard β-cyanoethyl phosphoramidite chemistry according to published protocols.[53,54] Specifically, the nucleoside ^{Fur}dG was converted into a phosphoramidite for use on a DNA synthesizer as per the synthetic strategy outlined in Scheme 1. The benzoheterocyclic series were incorporated into

Scheme 1. Synthesis of ^{Fur}dG Phosphoramidite

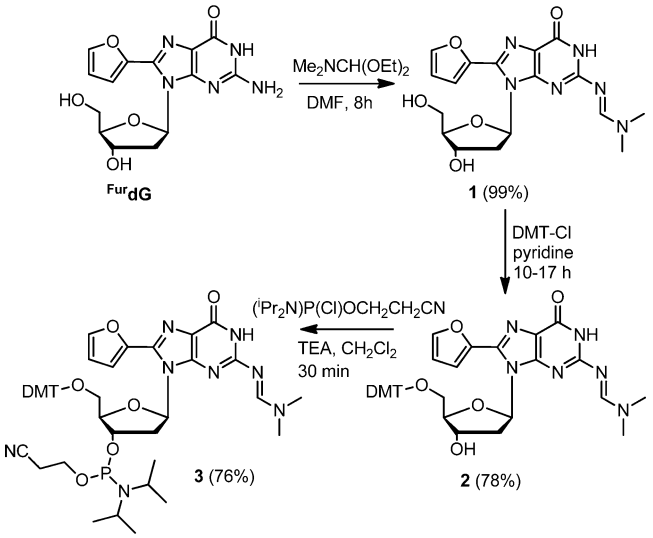

*Nar*I using our recently developed postsynthetic method[55] involving palladium (Pd)-catalyzed Suzuki−Miyaura coupling reactions with brominated *Nar*I oligonucleotides and 10 equiv of the requisite boronic acids. Negative electrospray ionization mass spectrometry (ESI-MS) analysis confirmed the identity of all C^8-heteroaryl-G modified oligonucleotides, synthesized by Suzuki−Miyaura coupling or standard phosphoramidite chemistry. The ESI-MS spectra showed the expected clusters of multiply charged peaks for the modified oligonucleotides, with the results of this analysis summarized in Table S8 (SI). Mass and UV spectra for all C^8-heteroaryl-G modified oligonucleotides, including MS spectra of the starting brominated *Nar*I oligonucleotide, are also included in the SI. Integration of HPLC traces[55] allowed for determination of yields from Suzuki−Miyaura couplings, which ranged from 10 to 21% (Table S8, SI).

UV Thermal Melting Studies. The C^8-heteroaryl-G modified oligonucleotides *Nar*I(X = ^{Fur}G, ^{Ind}G, ^{Bfur}G or ^{Bth}G) were hybridized to the complementary strand *Nar*I′(C) or *Nar*I′(G) (Figure 1). *Nar*I′(G) refers to the complementary strand in which a G has been inserted at the appropriate site to allow for positioning opposite the site of C^8-heteroaryl-G modification upon duplex formation. Our previous studies have shown C-linked C^8-aryl−dG adducts to stabilize the G:G mismatch,[40,42,55] and molecular dynamics (MD) simulations predict a *syn*-conformation for the modified C^8-dG adduct.[40,42]

dx.doi.org/10.1021/jo302164c | J. Org. Chem. 2012, 77, 10498−10508

In the present work, we determined the melting temperatures (T_m's) using UV−vis spectroscopy by monitoring the absorbance at 260 nm versus temperature, and results are summarized in Table 4.

Table 4. T_m Studies of C^8-Heteroaryl-G Modified *Nar*I Oligonucleotides Hybridized to *Nar*I′(C)[a] or *Nar*I′(G)[b]

duplex	T_m (°C)[c]	ΔT_m
*Nar*I(X = G):*Nar*I′(C)	60.5 ± 1.3	
*Nar*I(X = G):*Nar*I′(G)	49.6 ± 1.0	
*Nar*I(X = ^{Fur}G):*Nar*I′(C)	51.0 ± 0.9	−9.5
*Nar*I(X = ^{Fur}G):*Nar*I′(G)	56.8 ± 1.6	+7.2
*Nar*I(X = ^{Ind}G):*Nar*I′(C)	50.4 ± 2.6	−10.1
*Nar*I(X = ^{Ind}G):*Nar*I′(G)	55.3 ± 0.4	+5.7
*Nar*I(X = ^{Bfur}G):*Nar*I′(C)	48.7 ± 0.5	−11.8
*Nar*I(X = ^{Bfur}G):*Nar*I′(G)	57.5 ± 1.0	+7.9
*Nar*I(X = ^{Bth}G):*Nar*I′(C)	54.5 ± 1.0	−6.0
*Nar*I(X = ^{Bth}G):*Nar*I′(G)	55.2 ± 0.9	+5.6

[a] 5′-GATGGCGCCGAG. [b] 5′-GATGGGGCCGAG. [c] T_m's of duplexes (1.25 μM of each oligonucleotide) were measured in 50 mM sodium phosphate buffer, pH 7, with 0.1 M NaCl. Absorbance was monitored at 260 nm, with a heating rate of 1 °C min^{-1}.

In each instance, when the C^8-heteroaryl-G probe was paired with its normal pyrimidine partner C, the duplex was considerably destabilized, in the range from −6.0 to −11.8 °C, compared to the unmodified duplex. Clearly, these probes are perturbing and are not good emissive models for unmodified dG. In this regard, the results with X = ^{Fur}G were somewhat surprising because the relatively small furan ring was not expected to have such a destabilizing influence on duplex stability (ΔT_m = −9.5 °C). However, overall these findings are in agreement with previous studies showing that *C*-linked C^8-aryl-G (ΔT_m = −6 to −17 °C),[40,55] C^8-pyrenyl-G (ΔT_m ∼ −10 °C),[27] and *N*-linked C^8-arylamine-G (ΔT_m = −8 to −13 °C)[37] lesions significantly decrease duplex stability when paired with C, suggesting that the C^8-heteroaryl−dG adducts are reasonable emissive models of bulky adducts generated by chemical mutants.

For *N*-linked C^8-dG adducts base-paired with C, *anti*- and *syn*-conformations are in equilibrium and both are destabilizing.[29−32] In the *anti*-conformation, a major groove (B-type) structure is generated, placing the N-linked aryl ring system in the major groove. In the present case, this would result in exposure of the lipophilic C^8-heteroaryl moiety to the aqueous extrahelical environment and, subsequently, duplex destabilization and a decrease in T_m, compared to the unmodified duplex.[42] Additionally, steric clash between the major groove located C^8-heteroaryl substituent and the phosphate backbone and sugar moieties may be a factor in duplex destabilization.[26] By contrast, duplex destabilization could be the result of *syn*-conformer adaptation of the C^8-heteroaryl−dG adduct, which for N-linked C^8-dG adducts favors a stacked, intercalated (S-type) structure.[32−39] In this structure, the N-linked C^8-aryl moiety is intercalated between its flanking nucleobases, in turn flipping the opposing pyrimidine (C) out of the helix.[39] The resulting helical distortion and loss of W−C H-bonding accounts for the decreased duplex stability and decrease in T_m, compared to the unmodified duplex.[37] NMR evidence is in favor of the S-type structure for an N-linked heteroaryl adduct in *Nar*I at G_3.[39]

Interestingly, when the modified *Nar*I oligonucleotides were hybridized to the *Nar*I′(G) complement, thereby introducing a mismatch, the C^8-heteroaryl−dG adduct was observed to increase duplex stability, in the range of +5.6 to +7.2 °C, compared to the unmodified duplex. This stabilization effect was previously observed to occur with both phenolic[40] and benzothienyl[42] C^8-dG modified 10-mers, hybridized to the complement with G opposing the adduct, with observed increases in T_m of ∼+10 °C. These *C*-linked phenolic[40] and benzothienyl[42] C^8-dG modified duplexes, in addition to *N*-linked C^8-arylamine−dG modified duplexes,[34,36,38] are known to favor a wedge (W-type) motif, with the adduct in the *syn*-conformation, when the adduct is mismatched with a purine. In this conformation, the lipophilic C^8-heteroaryl moiety is located in the minor groove in a nonpolar environment, and is thus favorably protected from the aqueous environment surrounding the duplex. Duplex stabilization also comes as a result of an increase in π-stacking due to interactions between the modified base and its flanking bases and increases in the H-bonding stability as a result of additional interactions between the C^8-substituent and its base-pairing partner.[40,42]

Photophysical Studies. In order to definitively classify the C^8-heteroaryl−dG adducts as probes in the *Nar*I recognition sequence, their photophysical properties upon oligonucleotide incorporation were examined. Emission and excitation spectra of the adducted *Nar*I oligonucleotides in the single-strand state, and upon hybridization to the complementary strands *Nar*I′(C) and *Nar*I′(G) were obtained and are shown in Figure 4, with photophysical parameters given in Table 5.

While still fluorescent, all modified *Nar*I oligonucleotides exhibited significantly quenched emission intensity compared to the free C^8-heteroaryl−dG nucleosides, with relative emission intensity (I_{rel}) values of ∼0.05−0.06 (Table 5). Many fluorescent base analogues, including 2AP, exhibit quenched fluorescence when incorporated into DNA. For 2AP, several mechanisms have been proposed for fluorescence quenching that include base stacking effects,[56] photoinduced electron transfer,[57] and the presence of dark states.[58] Recent theoretical calculations reveal two different pathways that can lead to fluorescence quenching.[10] One involves conversion of the bright ($\pi\pi^*$) state into a dark minimum ($n\pi^*$) involving lone pair orbitals on 2AP. A second pathway involves charge transfer (CT) between the bases, which can lead to radiationless decay.

The wavelengths of emission for the modified oligonucleotides do not distinctly differ from those of the free nucleosides, with only very subtle shifts, or no change, in wavelength observed and no discernible pattern in the shift present (Table 5). The excitation spectra of the modified *Nar*I oligonucleotides did display other features distinct from the spectra of the free modified nucleosides. In all spectra, a new excitation band was present between ∼270 and 280 nm. In particular, this new band was clearly visible in the spectra of *Nar*I(X = ^{Ind}G) (Figure 4b, bold trace) and *Nar*I(X = ^{Bfur}G) (Figure 4c, bold trace). This peak occurs at the red-edge of DNA absorbance and can be ascribed to CT from the natural DNA nucleobases to the adduct.[42] Similar bands have been observed in the emission spectra of 2AP modified oligonucleotides, in the 260−270 nm region.[13,14] The wavelength of excitation of *Nar*I(X = ^{Ind}G) was considerably blue-shifted (15 nm) compared to the free nucleoside, suggesting a more twisted ^{Ind}G structure within *Nar*I.

dx.doi.org/10.1021/jo302164c | J. Org. Chem. 2012, 77, 10498−10508

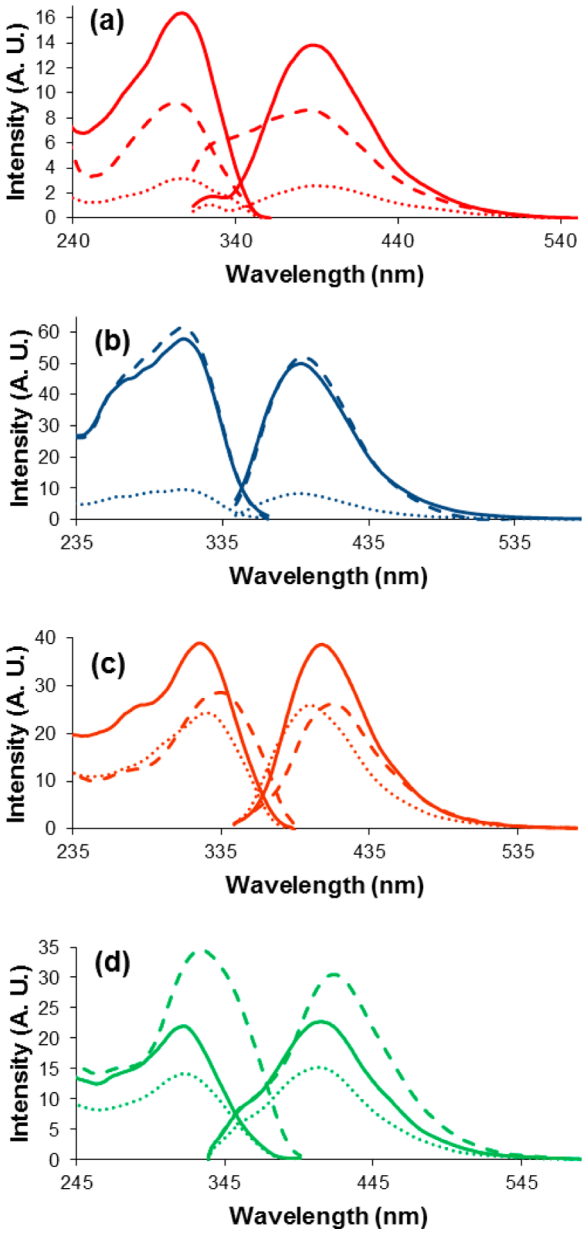

Figure 4. Excitation and emission spectra of C^8-heteroaryl-G modified *Nar*I oligonucleotides, in the single-strand state (solid line), or hybridized to its complementary strand, *Nar*I′(C) (dashed line) or *Nar*I′(G) (dotted line), with (a) *Nar*I(X = ^{Fur}G), (b) *Nar*I(X = ^{Ind}G), (c) *Nar*I(X = ^{Bfur}G) or (d) *Nar*I(X = ^{Bth}G). All spectra of single-strand oligonucleotides (1.25 μM) and duplexes (equivalent amounts (1.25 μM) of *Nar*I and its complementary strand) were recorded in 50 mM sodium phosphate buffer, pH 7, with 0.1 M NaCl at 10 °C.

The spectral changes upon hybridization were markedly different depending on the nature of the base opposing the probe in the duplex. For all modified *Nar*I oligonucleotides upon hybridization to *Nar*I′(C), an additional excitation band was observed at ~275 nm, as was observed in the excitation spectra of the single-strand oligonucleotides. Little change was observed in emission intensity, with I_{rel} values ranging from ~0.6−1.4, as compared to the single-strand oligonucleotide. The wavelength of emission for *Nar*I(X = ^{Ind}G), *Nar*I(X = ^{Bfur}G), and *Nar*I(X = ^{Bth}G) was notably red-shifted upon base-pairing to C, by increments of 2, 8, and 6 nm, respectively, compared to the single-strand oligonucleotides. This suggests

Table 5. Photophysical Parameters of C^8-Heteroaryl-G Modified *Nar*I Oligonucleotides Hybridized to *Nar*I′(C)[a] or *Nar*I′(G)[b]

oligonucleotide	λ_{ex} (nm)[a]	$\Delta\lambda_{ex}$ (nm)[b]	λ_{em} (nm)[a] (I_{rel})[c]	$\Delta\lambda_{em}$ (nm)[b]
*Nar*I(X = ^{Fur}G)	306	+2	386 (0.045)	+2
*Nar*I(X = ^{Fur}G):*Nar*I′(C)	305	−1	385 (0.63)	−1
*Nar*I(X = ^{Fur}G):*Nar*I′(G)	306		387 (0.18)	+1
*Nar*I(X = ^{Ind}G)	308	−15	389 (0.057)	−1
*Nar*I(X = ^{Ind}G):*Nar*I′(C)	308		391 (1.05)	+2
*Nar*I(X = ^{Ind}G):*Nar*I′(G)	307	−1	387 (0.17)	−2
*Nar*I(X = ^{Bfur}G)	320	−3	403 (0.060)	
*Nar*I(X = ^{Bfur}G):*Nar*I′(C)	335	+15	411 (0.67)	+8
*Nar*I(X = ^{Bfur}G):*Nar*I′(G)	325	+5	395 (0.62)	−8
*Nar*I(X = ^{Bth}G)	317	+2	413 (0.062)	−4
*Nar*I(X = ^{Bth}G):*Nar*I′(C)	328	+11	419 (1.41)	+6
*Nar*I(X = ^{Bth}G):*Nar*I′(G)	319	+2	408 (0.65)	−5

[a]All spectra of single-strand oligonucleotides (1.25 μM) and duplexes (equivalent amounts (1.25 μM) of *Nar*1 and its complementary strand) were recorded in 50 mM sodium phosphate buffer, pH 7, with 0.1 M NaCl at 10 °C. [b]Change in excitation or emission maximum for single-strand *Nar*1 is versus the free C^8-heteroaryl−dG adduct, while change for the duplex is versus single-strand *Nar*1. [c]I_{rel} for single-strand *Nar*1 is determined as $I_{single\text{-}strand}/I_{adduct}$. I_{adduct} was determined at a concentration of 1.25 μM. I_{rel} for the duplex is determined as $I_{duplex}/I_{single\text{-}strand}$. All intensity values for determination of I_{rel} were measured at the same wavelength.

that the modified bases are in a polar environment. Red-shifts in wavelength were also observed in the excitation spectra of *Nar*I(X = ^{Bfur}G):*Nar*I′(C) and *Nar*I(X = ^{Bth}G):*Nar*I′(C), of 15 and 11 nm, respectively. Negligible shifts in emission and excitation wavelengths were observed for the *Nar*I(X = ^{Fur}G):*Nar*I′(C) duplex, which may be indicative of a bulky C^8-moiety as a requirement of notable changes in fluorescence wavelength parameters, such as those observed for the *Nar*I oligonucleotides with ^{Ind}dG, ^{Bfur}dG, or ^{Bth}dG modifications.

By contrast, hybridization to the *Nar*I′(G) complement, and thereby induction of mismatch formation, resulted in different changes to the emission and excitation properties. The energy transfer assigned excitation band previously viewed for the single-strand oligonucleotides and *Nar*I′(C) hybridized duplexes was not observed, or was relatively indiscernible, in *Nar*I′(G)-hybridized duplexes. Furthermore, mismatch to the opposing G resulted in a decrease in emission intensity, as compared to the corresponding single-strand oligonucleotide with the largest decrease in intensity observed for the *Nar*I(^{Fur}G):*Nar*I′(G) and *Nar*I(^{Ind}G):*Nar*I′(G) duplexes, with I_{rel} = 0.18 and 0.17, respectively. It is of interest to note the decrease in degree of emission intensity correlates with decrease in intensity observed for the C^8-heteroaryl−dG nucleosides in going from water to the more viscous glycerol solvent (i.e., Figure 3) or to the more nonpolar $CHCl_3$ (Tables S1−S6, SI). A negligible shift in the wavelength of the fluorescence was again observed for the ^{Fur}G modified duplex, while the wavelength of emission for *Nar*I(^{Ind}G), *Nar*I(^{Bfur}G)

dx.doi.org/10.1021/jo302164c | J. Org. Chem. 2012, 77, 10498−10508

and *Nar*I(^{Bth}G) was blue-shifted upon mismatch formation, by increments of 2, 8, and 5 nm, respectively, compared to the single-strand oligonucleotides.

Collisional Fluorescence Quenching. Collisional fluorescence quenching studies provided further confirmation of adduct conformation in the duplex. Collisional quenching has proved useful for study of aqueous accessibility of fluorescent groups, with changes in sensitivity, exposure and accessibility following ligand binding indicative of a change in conformation of the fluorophore.[59] Collisional quenching, using quenchers such as acrylamide and deoxyuridine (neutral), iodide ion (negatively charged), and cesium ion (positively charged) has been used to provide insight into the conformation of proteins,[59,60] benzopyrene diol epoxide (BPDE)−DNA adducts[61] and 2AP.[62]

Collisional quenching experiments were first conducted with the free C^8-heteroaryl−dG adducts, using KI as quencher. Plots of F_o/F versus [KI] of the fluorescence quenching process of ^{Fur}dG (a) and *Nar*I(X = ^{Fur}G) hybridized to its complementary strand (b) *Nar*I′(C) or (c) *Nar*I′(G) are shown in Figure 5. Slopes of the plots derived from KI quenching experiments provide the Stern−Volmer quenching constant for different adducts, K_{sv}, which are listed in Table 6. Quenching constants reflect the extent of adduct accessibility toward the quencher.[62] Examination of the K_{sv} values determined for the quenching of modified duplexes by KI reveals that the values are much smaller than those determined for the corresponding adducts, reflecting a lower accessibility of the fluorophores to the quencher when located in the helical environment. The K_{sv} values also show that when base-paired to C, the fluorophore is more accessible to the aqueous environment than when mismatched to G, as larger K_{sv} values were derived for the modified oligonucleotides hybridized to *Nar*I′(C) than when hybridized to *Nar*I′(G).

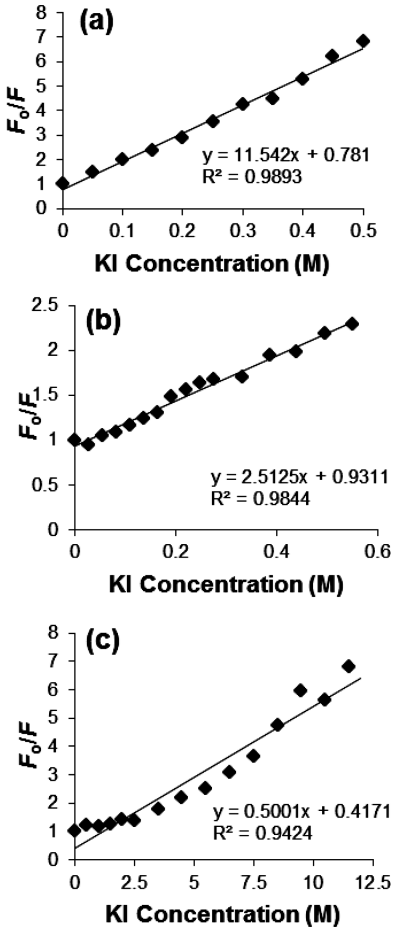

Figure 5. Plots of F_o/F vs [KI] for the collisional fluorescence quenching of (a) ^{Fur}dG and the C^8-heteroaryl-G modified oligonucleotide *Nar*I (X = ^{Fur}G) hybridized to its complementary strand (b) *Nar*I′(C) or (c) *Nar*I′(G). Spectra were recorded in 50 mM sodium phosphate, pH 7, with 100 mM NaCl, using 1.25 μM of the adduct or equivalent amounts (1.25 μM) of *Nar*I and its complementary strand. KI was added to the adduct sample in aliquots of 0.05 M and to the duplex samples in 0.025−1.0 M aliquots.

Table 6. Stern−Volmer Quenching Constants, K_{sv}, for Collisional Fluorescence Quenching of C^8-Heteroaryl−dG Adducts, or C^8-Heteroaryl-G Modified *Nar*I Oligonucleotides Hybridized to *Nar*I′(C) or *Nar*I′(G)

compd	K_{sv}[a] (M^{-1})
^{Fur}dG	10.2 ± 1.2
^{Bth}dG	11.8 ± 1.1
*Nar*I(X = ^{Fur}G):*Nar*I′(C)	2.51 ± 0.08
*Nar*I(X = ^{Fur}G):*Nar*I′(G)	0.50 ± 0.03
*Nar*I(X = ^{Bth}G):*Nar*I′(C)	2.5 ± 0.4
*Nar*I(X = ^{Bth}G):*Nar*I′(G)	0.64 ± 0.03

[a] K_{sv} values were determined from the slope of the plot of F_o/F vs [KI] (quencher concentration), expressed as values ± fitting error.

The T_m data for C^8-heteroaryl-G modified *Nar*I oligonucleotides hybridized to *Nar*I′(C) pointed toward two possible destabilizing adduct conformations; an *anti*-preferred conformation, with a B-type duplex motif, or a *syn*-preferred conformation with an S-type duplex motif. The K_{sv} values obtained following collisional quenching of *Nar*I′(C) annealed duplexes allows for a defining classification of the adduct conformation. The larger quenching constants for fluorescence quenching of *Nar*I(X = ^{Fur}G):*Nar*I′(C) and *Nar*I(X = ^{Bth}G):*Nar*I′(C) duplexes, compared to *Nar*I(X = ^{Fur}G):*Nar*I′(G), and *Nar*I(X = ^{Bth}G):*Nar*I′(G), can be equated to a more readily accessible fluorophore to the aqueous environment surrounding the double helix, and thus the quencher. In order for the fluorophores to be solvent exposed, the adduct must be in an *anti*-conformation, since in this conformation, the C^8-heteroaryl moiety is located outside of the helix in the major groove. From the corroboration of thermal melting, emission and excitation spectra, and finally collisional fluorescence quenching studies, the C^8-heteroaryl−G adduct likely exists in the *anti*-conformation when base-paired to C.

Conversely, the smaller slopes from plots of F_o/F versus [KI] determined from the quenching of *Nar*I(X = ^{Fur}G):*Nar*I′(G) and *Nar*I (X = ^{Bth}G):*Nar*I′(G) suggest that the fluorophore has become more shielded and is likely stacked within the interior of the helix. This implies a *syn*-preferred conformation for the C^8-heteroaryl−dG adduct upon mismatch formation, placing the C^8-heteroaryl moiety in a more rigid environment, which is also more nonpolar in nature. The solvatochromic, including viscosity-related, properties of the C^8-heteroaryl−dG adducts can account for its dramatic blue-shift and decrease in emission intensity upon base-pairing with G, and subsequently conversion of glycosyl bond conformation. This assumption is also consistent with the known *syn*-preference of N-linked adducts within a purine mismatch.[34,36,38]

dx.doi.org/10.1021/jo302164c | J. Org. Chem. 2012, 77, 10498−10508

CD Measurements. CD spectra of *Nar*I(X = ^{Fur}G) and *Nar*I(X = ^{BFur}G) hybridized to their complementary strands (a) *Nar*I′(C) or (b) *Nar*I′(G) are shown in Figures S7 and S8 (SI). The modified duplexes show characteristics of B-form DNA with roughly equal positive (275 nm) and negative (244 nm) bands and a crossover at ∼260 nm.[63] It was not possible to resolve ellipticities due to the C^8-heteroaryl-G modified bases, and so CD could not distinguish conformational preference by the adducts.

Selection of C^8-Heteroaryl−dG Probe for Future Studies. All C^8-heteroaryl−dG adducts described herein act as fluorescent nucleobase probes for selective excitation (306−320 nm) within the *Nar*I oligonucleotide (Table 5). DFT calculations indicate that the benzothienyl derivative ^{Bth}dG possesses the largest ground-state and excited-state dipole moment (Table 3) and its emission proved sensitive to conformation within the *Nar*I duplex structure. When base-paired with C (*Nar*I(X = ^{Bth}dG):NarI′(C), Table 5, Figure 4d), the ^{Bth}dG probe exhibited a red-shift of 6 nm and an increase in emission intensity 1.4-fold compared to the emission of the probe in the single-strand. In contrast, when base-paired with G (*Nar*I(X = ^{Bth}dG):NarI′(G)), the probe exhibited a blue-shift of 5 nm and exhibited quenched fluorescence compared to the probe emission in the single-strand. Overall, base-pairing with C provided a 2-fold increase in emission intensity and an 11 nm red-shift compared to the probe emission when base-paired with G. This change in emission characteristics was attributed to a change in conformation from *anti* to *syn*. The emission of the benzofuryl derivative ^{Bfur}dG was also sensitive to conformation on the basis of wavelength (16 nm difference, Table 5, Figure 4c), but not emission intensity. In contrast, the emission of the indole-linked derivative ^{Ind}dG was strongly quenched in the *syn*-conformation (I_{rel} = 0.17 compared to the single-strand), but it was not possible to distinguish base-pairing of ^{Ind}G with C from the single-strand *Nar*I, and the probe-incorporated duplexes failed to show changes in emission wavelength (Figure 4b). The smaller furyl derivative ^{Fur}dG exhibited quenched emission with both duplex structures with the emission wavelength lacking sensitivity to base-pairing. Thus, ^{Bth}dG was the only probe to show differences in both emission intensity and wavelength upon change in conformation within the *Nar*I duplex, making it the most sensitive probe for monitoring conformation. For mutagenic C^8-dG adducts, conformation within the DNA duplex is directly correlated with biological activity.[32−39] The ability to employ fluorescence spectroscopy to characterize adduct conformation should be useful for determining structure−activity relationships for adduct processing by the DNA polymerases.

EXPERIMENTAL SECTION

Materials and Methods. Boronic acids (1-*N*-Boc-pyrrole-2-, furan-2-, thiophene-2-, 1-*N*-Boc-indole-2-, benzofuran-2-, and thiophene-2-boronic acid), Pd(OAc)2, 3,3′,3″-phosphinidynetris(benzenesulfonic acid) trisodium salt (TPPTS), and other commercial compounds were used as received. The synthesis of 8-bromo-2′-deoxyguanosine (8-Br-dG) was performed according to literature procedures by treating dG with *N*-bromosuccinimide in water−acetonitrile.[64] Suzuki cross-coupling reactions of boronic acids with 8-Br-dG to afford ^{Pyr}dG,[41] ^{Fur}dG,[65] ThdG,[65] ^{Ind}dG,[41] ^{Bfur}dG,[66] and ^{Bth}dG[42,66] were performed as described previously by Western and co-workers.[67] NMR spectra were recorded on 300 and 600 MHz spectrometers in either DMSO-d_6, $CDCl_3$ or CD_3CN referenced to TMS (0 ppm) or the respective solvent. All UV−vis and fluorescence emission spectra were recorded with baseline correction and stirring using 10 mm light path quartz glass cells. Quantum yields for the nucleoside adducts were determined, as outlined previously in detail,[41] using the comparative method,[68] with quinine bisulfate (Φ_{fl} = 0.546 in 0.5 M H_2SO_4) serving as the fluorescence quantum yield standard.[69] pH measurements were taken at room temperature with stirring. Any water used for buffers or spectroscopic solutions was obtained from a filtration system (18.2 MΩ). High-resolution mass spectra were recorded on a Q-Tof instrument, operating in nanospray ionization at 0.5 uL/min detecting positive ions. Electrochemical oxidation measurements were conducted in a three-electrode glass cell under nitrogen in a solution of 0.1 M DMF/TBAF, as previously outlined in detail.[44−46]

Photophysical Properties of C^8-Heteroaryl−dG Adducts. Stock solutions were made in DMSO, due to sparing solubility in other solvents, to a concentration of 4 mM. Spectroscopic solutions of the modified nucleosides were prepared in 10 mM MOPS buffer, pH 7, with 100 mM NaCl, and made to a concentration of 50 μM for UV−vis measurements or 20 μM for fluorescence measurements. UV−vis spectra were recorded from 400 to 220 nm wavelength, using quartz cells (100-QS) with a light path of 10 mm. Fluorescence spectra were recorded at the excitation wavelength (absorbance maxima) for the C^8-heteroaryl−dG adducts, from 10 nm above the excitation wavelength to 600 nm. Fluorescence spectra were recorded using quartz cells (101-QS) with a light path of 10 × 10 mm, and excitation and emission slit widths were kept constant at 2.5 nm.

Oligonucleotide Synthesis by Standard Phosphoramidite Chemistry. Oligonucleotide synthesis for the C^8-heteroaryl-G modified *Nar*I oligonucleotide (5′-CTCGGCXCCATC) with X = ^{2Fur}G was carried out on a 1 μmol scale on a DNA synthesizer using standard β-cyanoethylphosphoramidite chemistry according to published protocols.[53,54] Following synthesis, oligonucleotides were cleaved from the solid support, deprotected using 2 mL of 30% ammonium hydroxide solution at 55 °C for 12 h and purified by HPLC.

*N^2-(Dimethylformamidyl)-8-(2″-furyl)-2′-deoxyguansine (**1**).* 8-(2″-Furyl)-2′-deoxyguansine (1.1 g, 3.3 mmol) was placed in 15 mL of dry DMF under argon. *N*,*N*-Dimethylformamide diethyl acetal (2.7 mL, 13.5 mmol) was then added and the mixture allowed to stir for 5 h. The reaction mixture was evaporated to dryness, washed with MeOH, and dried to give **1** as a gray solid (1.28 g, 99.0% yield): mp 195−197 °C; ^{1}H NMR (600.1 MHz, DMSO-d_6) δ 11.59 (s, 1H), 8.57 (s, 1H), 8.01 (d, *J* = 1.2 Hz, 1H), 7.07 (d, *J* = 3.3 Hz, 1H), 6.78 (dd, *J* = 1.8 Hz, 3.4 Hz, 1H), 6.51 (t, *J* = 7.2 Hz, 1H), 6.36 (d, *J* = 4.3 Hz, 1H), 4.95 (t, *J* = 5.1 Hz, 1H), 4.54 (m, 1H), 3.98 (m, 1H), 3.88 (m, 1H), 3.71 (m, 1H), 3.27 (m, 1H), 3.22 (s, 3H), 3.11 (s, 3H), 2.23 (m, 1H); ^{13}C NMR (151 MHz, DMSO-d_6) δ 159.2, 158.3, 158.0, 151.3, 145.6, 145.0, 139.8, 121.4, 113.3, 112.8, 88.6, 85.5, 71.9, 62.9, 41.8, 38.4, 35.6; HRMS calcd for $C_{17}H_{20}N_6O_5$ [M + H$^+$] 389.1573, found 389.1568.

*5′-O-(4,4′-Dimethoxytrityl)-N^2-(dimethylformamidyl)-8-(2″-furyl)-2′-deoxyguanosine (**2**).* 4,4′-Dimethoxytrityl chloride (DMT-Cl, 1.28 g, 3.78 mmol) was dissolved in 3 mL of dry pyridine. N^2-Dimethylformamide-8-(2″-furyl)-2′-deoxyguanosine **1** (923 mg, 2.70 mmol) was coevaporated from dry pyridine (3 × 5 mL) in a separate flask and reverse filled with argon. To this flask was added 7 mL of dry pyridine, followed by 3 mL of DMT-Cl/pyridine solution. The reaction was allowed to stir at room temperature for 3 h under argon and was monitored by TLC. Upon completion, the reaction mixture was diluted with ethyl acetate (10 mL) and washed with water (2 × 10 mL). To the washed reaction mixture was added 1 mL of triethylamine (TEA), and the mixture was then evaporated to dryness, with the resulting solid dissolved in CH_2Cl_2 (3 mL). Hexanes (10 mL) were added, and the reaction mixture was stirred overnight. The resulting suspension was filtered and purified on silica gel and eluted with MeOH/CH_2Cl_2/TEA (5:90:5) to afford **2** as a white solid (1.45 g, 78.0% yield): mp 162−167 °C; ^{1}H NMR (600.1 MHz, CD_3CN) δ 9.44 (bs, 1H), 8.33 (s, 1H), 7.66 (s, 1H) 7.29 (m, 2H), 7.16 (m, 7H), 7.06 (d, *J* = 3.4 Hz, 1H) 6.7 (m, 4H), 6.62 (dd, *J* = 1.62 Hz, 3.24 Hz, 1H), 6.50 (dd, *J* = 4.5 Hz, 8 Hz, 1H), 4.77 (q, *J* = 5.9 Hz, 13.0 Hz, 1H), 3.97 (m, 1H), 3.71 (s, 3H), 3.70 (s, 3H), 3.46 (m, 1H) 3.25 (m,

1H), 3.14 (m, 1H) 3.14 (s, 3H), 3.02 (s, 3H), 2.45 (q, J = 7.1 Hz, 14.3 Hz, 5H, TEA), 2.24 (m, 2H), 0.945 (t, J = 7.1 Hz, 8H, TEA); ^{13}C NMR (151 MHz, CD_3CN) δ 160.0, 159.9, 159.4, 158.9, 157.9, 152.1, 146.7, 146.3, 145.6, 141.5, 137.6, 137.4, 131.4, 131.1, 129.4, 129.1, 128.1, 122.2, 118.8 (CD_3CN), 114.3, 113.7, 113.2, 87.5, 87.1, 86.1, 72.9, 65.6, 56.32, 56.3, 47.5 (TEA), 42.2, 38.9, 35.7, 12.7 (TEA), 1.8 (CD_3CN); HRMS calcd for $C_{38}H_{38}N_6O_7$ [M + H$^+$] 691.2880, found 691.2866.

*3′-O-[(2-Cyanoethoxy)(diisopropylamino)phosphino]-5′-O-(4,4′-dimethoxytrityl)-N^2-(dimethylformamidyl)-8-(2″-furyl)-2′-deoxyguanosine (**3**).* 5′-DMT-N^2-dimethylformamide-8-(2″-furyl)-2′-deoxyguanosine **2** (0.25 g, 0.362 mmol) was coevaporated from dry toluene (3 × 5 mL). Dry CH_2Cl_2 (10 mL) was added to a reaction flask backfilled with argon. 2-Cyanoethyl *N*,*N*-diisopropylchlorophosphoramidite (0.14 mL, 0.398 mmol) was added to the flask along with 0.5 mL of dry TEA. The reaction was allowed to proceed to completion as monitored by TLC (90:5:5 CH_2Cl_2/MeOH/TEA). The reaction mixture was then reduced to dryness, immediately purified on silica gel, and eluted with 90:5:5 CH_2Cl_2/MeOH/TEA. The phosphoramidite **3** eluted as the diastereomers, which were a white foam (241 mg, 76.0%): ^{1}H NMR (600.1 MHz, $CDCl_3$) δ 9.28–9.24 (m, 1H), 8.32–8.27 (m, 1H), 7.44–7.06 (m, 13H), 6.66–6.56 (m, 5H), 6.43 (bs, 1H), 5.03–4.90 (m, 1H), 4.12 (m, 1H), 3.73–3.62 (m, 7H), 3.53–3.42 (m, 3H), 3.34–3.20 (m, 3H), 2.99 (s, 3H), 2.90 (s, 3H), 2.69–2.50 (m, 2H), 2.40–2.27 (m, 2H), 1.46 (m, 2H), 1.11–1.05 (m, 9H), 1.00–0.98 (m, 3H); ^{13}C NMR (151 MHz, $CDCl_3$) δ 158.32, 158.3, 157.7, 157.6, 157.5, 155.8, 155.8, 150.52, 150.50, 144.82, 144.80, 144.7, 143.60, 143.55, 140.39, 140.35, 135.82, 135.76, 135.7, 130.0, 129.9, 129.87, 128.1, 128.0, 127.7, 127.6, 126.7, 126.6, 121.1, 121.0, 117.6, 117.5, 112.93, 112.88, 112.85, 112.8, 111.73, 111.71, 86.04, 85.99, 84.9, 84.85, 84.78, 84.2, 83.9, 74.7, 74.5, 73.5, 73.4, 63.8, 63.3, 58.4, 58.3, 58.1, 58.0, 57,9, 55.2, 55.1,46.7, 45.2, 43.3, 41.1, 37.5, 35.1, 30.9, 29.2, 24.6, 24.5, 24.4, 24.3, 22.9, 22.8, 20.4, 20.2, 20.1; ^{31}P NMR (121.4 MHz, $CDCl_3$) δ 149.32, 148.93; HRMS calcd for $C_{47}H_{56}N_8O_8P$ [M + H]$^+$ 891.3959, found 891.3964.

Suzuki–Miyaura Coupling Reactions with 8-Br-G-modified Oligonucleotides. Synthesis of C^8-heteroaryl-G-modified *Nar*I oligonucleotides (5′-CTCGGCXCCATC) with X = ^{Ind}G, ^{Bfur}G, or ^{Bth}G was conducted using our recently developed postsynthetic Suzuki-Miyaura cross-coupling strategy.[55] The protocol is briefly described here. 8-Br-G-modified *Nar*I oligonucleotides (5′-CTCGGCXCCATC) with X = 8-Br-G were prepared on a 1 μmol scale using standard phosphoramidites and 8-Br-dG-CE phosphoramidite. The synthesized oligonucleotides were fully deprotected with ammonium hydroxide for 24 h, desalted, and purified by reversed-phase chromatography. The mass of *Nar*I(X = 8-Br-G) was rechecked prior to use in Suzuki–Miyaura coupling. For Suzuki–Miyaura coupling, *Nar*I(X = 8-Br-G) (500 nmol) was initially dissolved in degassed 2:1 H_2O/CH_3CN. The appropriate boronic acid and sodium carbonate were added to the solution at the molar ratios Ar-B$(OH)_2$/*Nar*I(X = 8-Br-G) = 10, and Na_2CO_3/*Nar*I(X = 8-Br-G) = 2. The other reaction components were initially prepared as 100× stock solutions in degassed water. Through serial dilution, the reagents were added to the reaction mixture at molar ratios *Nar*I(X = 8-Br-G)/TPPTS = 15, and *Nar*I(X = 8-Br-G)/Pd$(OAC)_2$ = 37.5, for a total volume of 700 μL 2:1 H_2O/CH_3CN, and the resulting solution was heated under argon at 80 °C for 24 h. To the reaction mixture was added 1 mL of 5 mM EDTA in 50 mM TEAA, pH 7.2. The resulting solution was added to a Sep-Pak Vac C18 1 cc cartridge and washed with 5% acetonitrile in 50 mM TEAA, pH 7.2 in order to remove excess reagents. The product was eluted with 30% acetonitrile in 50 mM TEAA, pH 7.2, and further purified by HPLC.

Oligonucleotide Purification and Sample Preparation. The C^8-heteroaryl-G-modified *Nar*I oligonucleotide solutions were first filtered using syringe filters (PVDF 0.20 μm), and concentrated under diminished pressure. Purification was performed using an HPLC instrument equipped with an autosampler, diode array detector (monitored at 258 nm and λ_{Abs} of the incorporated modified nucleoside), fluorescence detector (monitored at λ_{ex} and λ_{em} of the incorporated modified nucleoside), and autocollector. Separation was carried out at 50 °C using a 3 μm reversed-phase (RP) C18 column (50 × 4.60 mm) with a flow rate of 0.5 mL/min, and various gradients of buffer B in buffer A (buffer A = 95:5 aqueous 50 mM TEAA, pH 7.2/acetonitrile; buffer B = 30:70 aqueous 50 mM TEAA, pH 7.2/acetonitrile. Yields were determined from integration of the HPLC trace.[55] Collected DNA samples were lyophilized to dryness and unmodified and C^8-heteroaryl-G modified *Nar*I oligonucleotides were dissolved in 18.2 MΩ water for quantification by UV–vis measurement using ε_{260}. Extinction coefficients were obtained from the following website: http://www.idtdna.com/analyzer/applications/oligoanalyzer. The C^8-heteroaryl-G modified *Nar*I oligonucleotides were assumed to have the same extinction coefficient as the natural *Nar*I oligonucleotide.[55] In all cases of hybridization, oligonucleotides were annealed by heating at 80 °C for 10 min, cooling to room temperature, and refrigerating until analysis.

MS Analysis of Oligonucleotides. Oligonucleotide samples were prepared in 50:50 methanol/water containing 0.1 mM ammonium acetate. Full scan MS spectra were obtained by direct infusion at a rate of 5–10 μL/min into an ESI source operated in negative mode and analyzed using triple quadrupole mass spectrometers. The capillary and cone voltages were optimized for each analyte and varied from 2.5 to 3.5 kV and 25–35 V, respectively. A source offset of 60 V was used for all samples. The desolvation temperature was between 250 and 350 °C. All data was acquired with 36–60 MCA and processed using mass spectrometry software.

Thermal Melting. All melting temperatures (T_m's) of oligonucleotides were measured by UV–vis spectroscopy in 50 mM phosphate buffer, pH 7, with 100 mM NaCl, using equivalent amounts (1.25 μM) of the unmodified or C^8-heteroaryl-G modified *Nar*I oligonucleotide and its complementary strand. The UV absorption at 260 nm was monitored as a function of temperature using quartz cells (108.002-QS) with a light path of 10 mm. The temperature was increased from 10 to 80 °C, or decreased from 80 to 10 °C, at a heating rate of 1 °C/min. The T_m's of the duplexes were calculated by determining the first derivative of the melting curve.

Circular Dichroism Measurements. Spectra were obtained on a CD spectrophotometer equipped with a 1 × 6 multicell block thermal controller and a water circulator unit. Measurements were carried out in 50 mM phosphate buffer, pH 7, with 100 mM NaCl, using equivalent amounts (1.25 μM) of the unmodified or C^8-heteroaryl-G-modified *Nar*I oligonucleotide and its complementary strand. Quartz glass cells (110-QS) with a light path of 1 mm were used for measurements. Spectra were collected at 10 °C between 200 and 400 nm, with a bandwidth of 1 nm and scanning speed at 100 nm/min. Each oligonucleotide sample was scanned nine times and background corrected.

Fluorescence Studies of C^8-Heteroaryl-G Modified *Nar*I Oligonucleotides. All fluorescence spectra were recorded in 50 mM phosphate buffer, pH 7, with 100 mM NaCl. In each case, both excitation and emission spectra were recorded for the C^8-heteroaryl-G modified *Nar*I oligonucleotide hybridized to its complementary strand. In addition, to allow for comparison, spectra were recorded for the C^8-heteroaryl–dG nucleoside adducts under the same conditions. All adduct and single-strand oligonucleotide samples were prepared to a final concentration at 1.25 μM, and duplex samples were prepared using equivalent amounts (1.25 μM) of the C^8-heteroaryl-G modified *Nar*I oligonucleotide and its complementary strand. All measurements were made using quartz cells (108.002F-QS) with a light path of 10 × 2 mm, and excitation and emission slit-widths were kept constant at 5 nm. All fluorescence excitation spectra were recorded at the emission wavelength (maximum) of the C^8-heteroaryl–dG adduct, from 200 to 10 nm below the emission wavelength, while fluorescence emission spectra were recorded at the excitation wavelength (maximum) of the adduct, from 10 nm above the excitation wavelength to 600 nm. Spectra were initially recorded at 10 °C and then at increasing 10 °C intervals to a maximum of 80 °C. Samples were held at each temperature for 5 min prior to beginning measurement.

Collisional Fluorescence Quenching Studies. All quenching studies were carried out using KI as the quencher, following a previously described method.[59] A 5 M stock solution of KI was

prepared in 50 mM sodium phosphate, pH 7, with 100 mM NaCl, and 0.1 mM $Na_2S_2O_3$ was added to the stock solution to prevent I_3^- formation. Fluorescence measurements were carried out in 50 mM sodium phosphate, pH 7, with 100 mM NaCl using 1.25 μM of the C^8-heteroaryl–dG adduct, or equivalent amounts (1.25 μM) of the C^8-heteroaryl-G modified *Nar*I oligonucleotide and its complementary strand. KI was added to the duplex sample as 0.025 or 0.05 M aliquots. All measurements were made at 10 °C using quartz cells (108.002F-QS) with a light path of 10 × 2 mm, and excitation and emission slit-widths were kept constant at 5 nm. Fluorescence emission intensity was measured at the emission wavelength maximum for the corresponding C^8-heteroaryl–dG adduct. Quenching data for the homogeneous single fluorophores system were analyzed using the Stern–Volmer equation

$$F_o/F = 1 + K_{sv}[Q]$$

where F_o and F are the fluorescence intensities in the absence and presence of the quencher, respectively, [Q] is the concentration of the quencher, KI, and K_{sv} is the Stern–Volmer quenching constant. Values for K_{sv} were determined from the slope of F_o/F versus [Q].

DFT Calculations. The preferred conformations of the ^{Pyr}dG adduct were previously analyzed by scanning the potential energy surface (PES) with respect to rotation about θ, the dihedral angle controlling the relative orientation of the heterocyclic ring at the C^8-position and the nucleobase ring, and χ, the dihedral angle controlling the orientation of the nucleobase about the glycosidic bond (Figure 1).[41] Full optimizations were subsequently carried out to identify minima and transition states on PES.

In the present work, all minima and transition states previously identified for the ^{Pyr}dG adduct[41] were used to generate the initial conformations of the adducts analyzed in the present work. Specifically, the pyrrole ring of ^{Pyr}dG was replaced with a furan, thiophene, indole, benzofuran or benzothiophene ring to generate ^{Fur}dG, ThdG, ^{Ind}dG, ^{Bfur}dG, and ^{Bth}dG adducts, respectively. Since the *anti* minima of ^{Pyr}dG are at least 25 kJ/mol higher in energy than the global *syn* minima, it is anticipated that all *anti* minima will be higher in energy compared to *syn* minima for all adducts analyzed in the present work. Therefore, only the *syn* minima and transition states were considered for the adducts analyzed in the present work. These conformations of the adducts were optimized at the B3LYP/6-31G(d) level of theory.

Higher level (B3LYP/6-311+G(2df,p)) single-point as well as B3LYP/6-31G(d) frequency calculations were performed on all fully optimized structures for the nucleoside models, and scaled zero-point vibrational energies (ZPVE) are included in the reported relative energies. The global minimum identified for each nucleoside adduct was used to calculate the B3LYP/6-31G(d) orbital energies and TD-B3LYP/6-31G(d) vertical excitation energies. Geometry optimizations of the first excited singlet state (S_1 state) of the adducts were carried out with CIS/6-31G(d) using the global minimum of the ground state as starting geometries. All electronic structure calculations were performed using Gaussian 09.[70]

■ ASSOCIATED CONTENT

Supporting Information

Figures S1–S8 and Tables S1–S8 described in the text, NMR spectra of synthetic samples, UV and ESI-MS spectra of modified *Nar*I oligonucleotides, and Tables S9–S20 (Cartesian coordinates of global minimum S_0 geometries and S_1 excited-state geometries of nucleoside adducts). This material is available free of charge via the Internet at http://pubs.acs.org.

■ AUTHOR INFORMATION

Corresponding Author

*E-mail: (S.D.W.) stacey.wetmore@uleth.ca, (R.A.M.) rmanderv@uoguelph.ca.

Notes

The authors declare no competing financial interest.

■ ACKNOWLEDGMENTS

Financial support for this research was provided by the Natural Sciences and Engineering Research Council (NSERC) of Canada, the Canada Research Chairs program, the Canada Foundation for Innovation, and the Ontario Innovation Trust Fund. This research has been facilitated by use of computing resources provided by WestGrid and Compute/Calcul Canada. We wish to thank Prof. Scott Mabury for providing use of the MS facilities at University of Toronto. A helpful discussion with Prof. Robert Hudson (University of Western Ontario) is also acknowledged.

■ REFERENCES

(1) Wilson, J. N.; Kool, E. T. *Org. Biomol. Chem.* **2006**, *4*, 4265–4274.
(2) Sinkeldam, R. W.; Greco, N. J.; Tor, Y. *Chem. Rev.* **2010**, *110*, 2579–2619.
(3) El-Sagheer, A. H.; Brown, T. *Chem. Soc. Rev.* **2010**, *39*, 1388–1405.
(4) Vineyard, D.; Zhang, X.; Donnelly, A.; Lee, I.; Berdis, A. J. *Org. Biomol. Chem.* **2007**, *5*, 3623–3630.
(5) Okamoto, A.; Tanaka, K.; Fukuta, T.; Saito, I. *J. Am. Chem. Soc.* **2003**, *125*, 9296–9297.
(6) Hendrickson, C. L.; Devine, K. G.; Benner, S. A. *Nucleic Acids Res.* **2004**, *32*, 2241–2250.
(7) Jhaveri, S.; Rajendran, M.; Ellington, A. D. *Nat. Biotechnol.* **2000**, *18*, 1293–1297.
(8) Deleavey, G. F.; Damha, M. J. *Chem. Biol.* **2012**, *19*, 937–954.
(9) Xu, D.; Evans, K. O.; Nordlund, T. M. *Biochemistry* **1994**, *33*, 9592–9599.
(10) Liang, J.; Matsika, S. *J. Am. Chem. Soc.* **2011**, *133*, 6799–6808.
(11) Stivers, J. T. *Nucleic Acids Res.* **1998**, *26*, 3837–3844.
(12) Hariharan, C.; Reha-Krantz, L. J. *Biochemistry* **2005**, *44*, 15674–15684.
(13) Nordlund, T. M.; Xu, D.; Evans, K. O. *Biochemistry* **1993**, *32*, 12090–12095.
(14) O'Neill, M. A.; Barton, J. K. *J. Am. Chem. Soc.* **2002**, *124*, 13053–13066.
(15) Dodd, D. W.; Hudson, R. H. E. *Mini-Rev. Org. Chem* **2009**, *6*, 378–391.
(16) Wilhelmsson, L. M. *Q. Rev. Biophys.* **2010**, *43*, 159–183.
(17) Wilhelmsson, L. M.; Holmén, A.; Albinsson, B.; Nordén, B. *J. Am. Chem. Soc.* **2001**, *123*, 2434–2435.
(18) Sandin, P.; Börjesson, K.; Li, H.; Mårtensson, J.; Brown, T.; Wilhelmsson, L. M.; Albinsson, B. *Nucleic Acids Res.* **2008**, *36*, 157–167.
(19) Börjesson, K.; Preus, S.; El-Sagheer, A. H.; Brown, T.; Albinsson, B.; Wilhelmsson, L. M. *J. Am. Chem. Soc.* **2009**, *131*, 4288–4293.
(20) Wojciechowski, F.; Hudson, R. H. E. *J. Am. Chem. Soc.* **2008**, *130*, 12574–12575.
(21) Srivatsan, S.; Tor, Y. *J. Am. Chem. Soc.* **2007**, *129*, 2044–2053.
(22) Pawar, M. G.; Srivatsan, S. G. *Org. Lett.* **2011**, *13*, 1114–1117.
(23) Millen, A. L.; McLaughlin, C. K.; Sun, K. M.; Manderville, R. A.; Wetmore, S. D. *J. Phys. Chem. A* **2008**, *112*, 3742–3753.
(24) Ben Gaied, N.; Glasser, N.; Ramalanjaona, N.; Beltz, H.; Wolff, P.; Marquet, R.; Burger, A.; Mély, Y. *Nucleic Acids Res.* **2005**, *33*, 1031–1039.
(25) Nadler, A.; Strohmeier, J.; Diederichsen, U. *Angew. Chem., Int. Ed.* **2011**, *50*, 5392–5396.
(26) Dierckx, A.; Diner, P.; El-Sagheer, A.; Kumar, J. D.; Brown, T.; Grotli, M.; Wilhelmsson, L. M. *Nucleic Acids Res.* **2011**, *39*, 4513–4520.

(27) Wanninger-Weifl, C.; Valis, L.; Wagenknecht, H.-A. *Bioorg. Med. Chem.* **2008**, *16*, 100−106.
(28) Dumas, A.; Luedtke, N. W. *J. Am. Chem. Soc.* **2010**, *132*, 18004−18007.
(29) Dumas, A.; Luedtke, N. W. *Nucleic Acids Res.* **2011**, *39*, 6825−6834.
(30) Manderville, R. A. Structural and Biological Impact of Radical Addition Reactions with DNA Nucleobases. In *Advances in Physical Organic Chemistry*; Richard, J. P., Ed.; Elsevier: Oxford, 2009; Vol. *43*, pp 177−218.
(31) Manderville, R. A. DNA Damage by Phenoxyl Radicals. In *Radical and Radical Ion Reactivity in Nucleic Acid Chemistry*; Greenberg, M., Ed.; John Wiley and Sons: Hoboken, NJ, 2009; Vol. *14*, pp 421−443.
(32) Patel, D. J.; Mao, B.; Gu, Z.; Hingerty, B. E.; Gorin, A.; Basu, A. K.; Broyde, S. *Chem. Res. Toxicol.* **1998**, *11*, 391−407.
(33) Stover, J. S.; Chowdhury, G.; Zang, H.; Guengerich, F. P.; Rizzo, C. J. *Chem. Res. Toxicol.* **2006**, *19*, 1506−1517.
(34) Cho, B. Structure−Function Characteristics of Aromatic Amine−-DNA Adducts. In *The Chemical Biology of DNA Damage*; Geacintov, N. E., Broyde, S., Eds.; Wiley-VCH: New York, 2010; pp 217−238.
(35) Hoffmann, G. R.; Fuchs, R. P. P. *Chem. Res. Toxicol.* **1997**, *10*, 347−359.
(36) Liang, F.; Meneni, S.; Cho, B. P. *Chem. Res. Toxicol.* **2006**, *19*, 1040−1043.
(37) Elmquist, C. E.; Wang, F.; Stover, J. S.; Stone, M. P.; Rizzo, C. J. *Chem. Res. Toxicol.* **2007**, *20*, 445−454.
(38) Zhou, L.; Rajabzadeh, M.; Traficante, D. D.; Cho, B. P. *J. Am. Chem. Soc.* **1997**, *119*, 5384−5389.
(39) Wang, F.; DeMuro, N.; Elmquist, C.; Stover, J. S.; Rizzo, C. J.; Stone, M. *J. Am. Chem. Soc.* **2006**, *128*, 10085−10095.
(40) Omumi, A.; Millen, A. L.; Wetmore, S. D.; Manderville, R. A. *Chem. Res. Toxicol.* **2011**, *24*, 1694−1709.
(41) Schlitt, K. M.; Millen, A. L.; Wetmore, S. D.; Manderville, R. A. *Org. Biomol. Chem.* **2011**, *9*, 1565−1571.
(42) Manderville, R. A.; Omumi, A.; Rankin (née Schlitt), K. M.; Wilson, K. A.; Millen, A. L.; Wetmore, S. D. *Chem. Res. Toxicol.* **2012**, *25*, 1271−1282.
(43) Onidas, D.; Markovitsi, D.; Marguet, S.; Sharonov, A.; Gustavsson, T. *J. Phys. Chem. B* **2002**, *106*, 11367−11374.
(44) Sun, K. M.; McLaughlin, C. K.; Lantero, D. R.; Manderville, R. A. *J. Am. Chem. Soc.* **2007**, *129*, 1894−1895.
(45) Weishar, J. L.; McLaughlin, C. K.; Baker, M.; Gabryelski, W.; Manderville, R. A. *Org. Lett.* **2008**, *10*, 1839−1842.
(46) Witham, A. A.; Beach, D. G.; Gabryelski, W.; Manderville, R. A. *Chem. Res. Toxicol.* **2012**, *25*, 315−325.
(47) Jamison, J. L.; Davenport, L.; Williams, B. W. *Chem. Phys. Lett.* **2006**, *422*, 30−35.
(48) Millen, A. L.; Manderville, R. A.; Wetmore, S. D. *J. Phys. Chem. B* **2010**, *114*, 4373−4382.
(49) Butler, R. S.; Cohn, P.; Tenzel, P.; Abboud, K. A.; Castellano, R. K. *J. Am. Chem. Soc.* **2009**, *131*, 623−633.
(50) Maus, M.; Rettig, W.; Bonafoux, D.; Lapouyade, R. *J. Phys. Chem. A* **1999**, *103*, 3388−3401.
(51) Sharafy, S.; Muszkat, K. A. *J. Am. Chem. Soc.* **1971**, *93*, 4119−4125.
(52) Greco, N. J.; Tor, Y. *Tetrahedron* **2007**, *63*, 3515−3527.
(53) Viazovkina, E.; Mangos, M. M.; Elzagheid, M. I.; Damha, M. J. *Curr. Protoc. Nucleic Acid Chem.* **2002**, Chapter 4, Unit 15.
(54) Vongsutilers, V.; Daft, J. R.; Shaughnessy, K. H.; Gannett, P. M. *Molecules* **2009**, *14*, 3339−3352.
(55) Omumi, A.; Beach, D. G.; Gabryelski, W.; Manderville, R. A. *J. Am. Chem. Soc.* **2011**, *133*, 42−50.
(56) Rachofsky, E. L.; Osman, R.; Ross, J. B. A. *Biochemistry* **2001**, *40*, 946−956.
(57) Wan, C.; Fiebig, T.; Schiemann, O.; Barton, J.; Zewail, A. *Proc. Natl. Acad. Sci. U.S.A.* **2000**, *97*, 14052−14055.
(58) Somsen, O. J. G.; Keukens, L. B.; Niels de Keijzer, M.; van Hoek, A.; van Amerongen, H. *ChemPhysChem* **2005**, *6*, 1622−1627.
(59) Siarheyeva, A.; Liu, R.; Sharom, F. J. *J. Biol. Chem.* **2010**, *285*, 7575−7586.
(60) Liu, R.; Lu, P.; Chu, J. W. K.; Sharom, F. J. *J. Biol. Chem.* **2008**, *284*, 1840−1852.
(61) Huang, W.; Amin, S.; Geacintov, N. E. *Chem. Res. Toxicol.* **2002**, *15*, 118−126.
(62) Jain, N.; Reshetnyak, Y. K.; Gao, L.; Chiarelli, M. P.; Cho, B. P. *Chem. Res. Toxicol.* **2008**, *21*, 445−452.
(63) Gray, D. M.; Ratliff, R. L.; Vaughan, M. R. *Methods Enzymol.* **1992**, *211*, 389−406.
(64) Gillet, L.; Schärer, O. D. *Org. Lett.* **2002**, *4*, 4205−4208.
(65) Dumas, A.; Luedtke, N. W. *Chem.—Eur. J.* **2011**, *18*, 245−254.
(66) Hobley, G.; Gubala, V.; Rivera-Sanchez, Del C.; Rivera, M. J. M. *Synlett* **2008**, *10*, 1510−1514.
(67) Western, E. C.; Daft, J. R.; Johnson, E. M., II; Gannett, P. M.; Shaughnessy, K. H. *J. Org. Chem.* **2003**, *68*, 6767−6774.
(68) Fery-Forgues, S.; Lavabre, D. *J. Chem. Educ.* **1999**, *76*, 1260−1264.
(69) Demas, J. N.; Crosby, G. A. *J. Phys. Chem.* **1971**, *75*, 991−1024.
(70) Gaussian 09, Revision A.1: Frisch, M. J.; Trucks, G. W.; Schlegel, H. B.; Scuseria, G. E.; Robb, M. A.; Cheeseman, J. R.; Scalmani, G.; Barone, V.; Mennucci, B.; Petersson, G. A.; Nakatsuji, H.; Caricato, M.; Li, X.; Hratchian, H. P.; Izmaylov, A. F.; Bloino, J.; Zheng, G.; Sonnenberg, J. L.; Hada, M.; Ehara, M.; Toyota, K.; Fukuda, R.; Hasegawa, J.; Ishida, M.; Nakajima, T.; Honda, Y.; Kitao, O.; Nakai, H.; Vreven, T.; Montgomery, J. A., Jr.; Peralta, J. E.; Ogliaro, F.; Bearpark, M.; Heyd, J. J.; Brothers, E.; Kudin, K. N.; Staroverov, V. N.; Kobayashi, R.; Normand, J.; Raghavachari, K.; Rendell, A.; Burant, J. C.; Iyengar, S. S.; Tomasi, J.; Cossi, M.; Rega, N.; Millam, N. J.; Klene, M.; Knox, J. E.; Cross, J. B.; Bakken, V.; Adamo, C.; Jaramillo, J.; Gomperts, R.; Stratmann, R. E.; Yazyev, O.; Austin, A. J.; Cammi, R.; Pomelli, C.; Ochterski, J. W.; Martin, R. L.; Morokuma, K.; Zakrzewski, V. G.; Voth, G. A.; Salvador, P.; Dannenberg, J. J.; Dapprich, S.; Daniels, A. D.; Farkas, Ö.; Foresman, J. B.; Ortiz, J. V.; Cioslowski, J.; Fox, D. J. Gaussian, Inc., Wallingford, CT, 2009.